Workspace Analysis and Optimal Design of a 3-Leg 6-DOF Parallel Platform Mechanism

Bruno Monsarrat and Clément M. Gosselin, *Member, IEEE*

***Abstract*—A new class of six-degree-of-freedom (DOFs) spatial parallel platform mechanism is considered in this paper. The architecture consists of a mobile platform connected to the base by three identical kinematic chains using five-bar linkages. Recent investigations showed that parallel mechanisms with such a topology for the legs can be efficiently statically balanced using only light elastic elements. This paper follows up with a workspace analysis and optimization of the design of that parallel mechanism. More specifically, considering a possible industrial application of the architecture as a positioning and orienting device of heavy loads, an optimization procedure for the maximization of the volume of the three-dimensional (3-D) constant-orientation workspace of the mechanism is first presented. As the mechanism could also have great potential as a motion base for flight simulators, we develop here a discretization method for the computation and graphical representation of a new workspace with coupled translational and rotational DOFs. This workspace can be defined as the 3-D space which can be obtained when generalized coordinates x, y and torsion angle ψ in the tilt-and-torsion angles parametrization are constant. A second procedure is then presented for the maximization of the volume of this second subset of the complete workspace. For both approaches, our purpose is to attempt an optimal design of the mechanism by maximizing the volume of the associated 3-D Cartesian region that is free of critical singularity loci.**

***Index Terms*—Design, optimization, parallel manipulator, singularity-free workspace.**

I. Introduction

DUE TO THEIR properties of increased nominal load-to-weight ratio, structural rigidity, positioning accuracy, and dynamic performances, parallel mechanisms have been extensively studied over the last 30 years (see [28] for a detailed review on parallel robots). Moreover, during the past decade, they have started to receive considerable attention by manufacturers, finding various commercial applications such as motion simulators, milling machines, assembly cells, and many others. However, in industrial applications of such mechanisms, where displacements of heavy loads are involved, the size of the actuators and the inherent operating costs are increased substantially. This motivated the development of parallel architectures that can be statically balanced. A mechanism is statically balanced if its potential energy is constant for all possible configurations, i.e., zero actuator forces/torques are required whenever the manipulator is at rest in any configuration. To the knowledge of the authors, static balancing of spatial six-degree-of-freedom (DOF) parallel manipulators was first introduced in [18], [19], [34], and [35]. Two static balancing methods, namely, counterweights and springs, were used. Moreover, [10] presented a class of spatial parallel platform mechanisms of novel architecture that is suitable for static balancing. The particular morphology of the kinematic chains connecting the base to the mobile platform (referred to as *legs* in this paper), based on five-bar linkages and similar to what was used in [33], allows an efficient static balancing using only springs. The sufficient conditions on the kinematic parameters that guarantee static balancing were derived for that class. A prototype with three identical legs was designed in [17] in accordance with the static balancing-related constraints (see Fig. 1). The figure illustrates the actuation scheme chosen for the prototype.

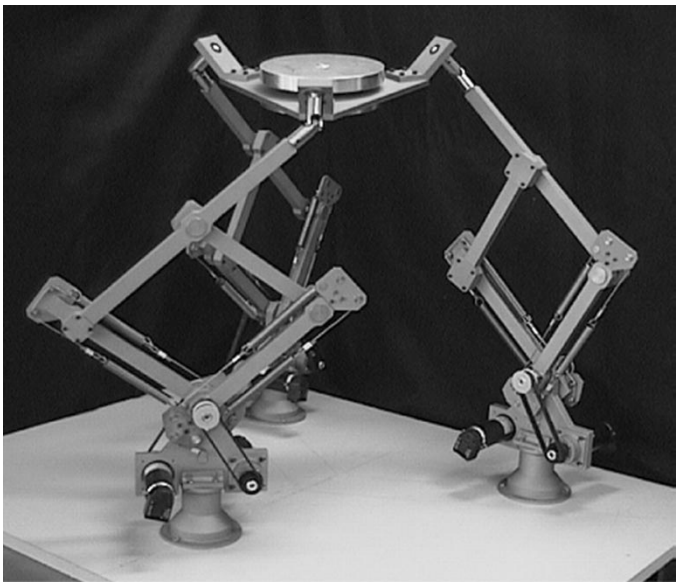

Fig. 1. Initial prototype of the three-leg statically balanced 6-DOF parallel platform mechanism (built in [17]).

Subsequently, a kinematic study of that mechanism class was presented in [9]. An analytical formulation for the inverse kinematics was presented and an expression of the Jacobian matrix was obtained in a general form. Closed-form expressions for the singularity loci were also determined for a second case of actuation, namely, for the case where the rotation angle around the vertical axis and the angle between the two proximal links of the parallelogram are actuated for each leg. In addition, [29] recently

Manuscript received October 9, 2001; revised September 12, 2002. This paper was recommended for publication by Associate Editor M. Shoham and Editor I. Walker upon evaluation of the reviewers' comments. This work was supported under research grants from the Natural Sciences and Engineering Research Council of Canada (NSERC).

B. Monsarrat is with the Aerospace Manufacturing Technology Centre, NRC Institute for Aerospace Research, Montreal, QC H4T 1W5, Canada (e-mail: Bruno.Monsarrat@cnrc-nrc.gc.ca).

C. M. Gosselin is with the Department of Mechanical Engineering, Laval University, Quebec City, QC G1K 7P4, Canada (e-mail: gosselin@gmc.ulaval.ca).

Digital Object Identifier 10.1109/TRA.2003.819603

presented a singularity analysis of this three-leg 6-DOF parallel mechanism using Grassmann line geometry. In the latter reference, the Jacobian matrix was determined in a very compact form using the principle of virtual work, and closed-form expressions were obtained for the singularity loci of the mechanism with an actuation scheme identical to what was used for the previously described prototype. References [21] and [22] also presented the design of a small-scale prototype with four legs, and discussed the critical issues for the practical implementation of a statically balanced 6-DOF parallel platform mechanism. These recent works also addressed the kinematic design of such an architecture via a maximization of the approximated volume of the constant-orientation workspace, defined as the set of all positions that can be attained by a reference point of the mobile platfom when the latter is kept at a constant orientation, the workspace being computed using the geometric approach proposed in [13].

Subsequently, when the kinematic synthesis of parallel mechanisms comes into practice, it appears that several approaches have been proposed in the literature. In the first approach, optimum characteristics are obtained by resorting to three criteria, namely: 1) symmetry considerations; 2) the maximization of the volume of the associated workspace; and 3) the minimization of the condition number of the Jacobian matrix in order to achieve a design as close to kinetostatic isotropy as possible ([11], [12], [16], and [24]). A weighted combination of these criteria combined with a minimization of the global dexterity index [14] was recently used in [2] to enhance the kinematic performances of a parallel 3-DOF spherical haptic device. Some authors have also investigated the parameter design of spatial parallel manipulators whose workspace has to include a prescribed volume. The latter design criterion was implemented using the following major approaches, namely: 1) in [5] and [6] by solving an optimization problem using genetic algorithms; 2) in [27] by solving the equations of the inverse kinematics for a set of design parameters and then by computing the suitable intersections between the allowable regions associated with the leg lengths, the range of motion of the passive joints, and the leg interferences; 3) by defining the objective complete workspace by a set of points in the six-dimensional (6-D) space for which the optimum values of the design parameters are solved using an analytical formulation for the direct and inverse kinematics [7]; and 4) by using a constrained optimization scheme to ensure that the workspace volume is as close as possible to a specified volume ([30] and [31]). Another criterion for optimum kinematic design consists of the synthesis of a parallel mechanism whose prescribed workspace is free of singularities [32].

In this paper, we address the parameter design of the three-leg statically balanced 6-DOF parallel manipulator shown in Fig. 1. This initial version of the mechanism was designed considering a unique design criterion, i.e., the fulfillment of the static balancing-related constraints. In spite of feasible design characteristics being determined, it appeared that the kinematic performances of the resulting mechanism were not satisfactory, viz.: 1) its workspace capability was limited; 2) it was shown in [29] that its workspace contains singularity surfaces that have a critical impact on the set of Cartesian points that are reachable in practice by the end-effector; and 3) the initial version of the manipulator had been inopportunely designed such that its workspace was divided into two connected regions separated by a critical singular configuration corresponding exactly to its neutral position (a singularity occurs when the mobile platform is parallel to the base and rotated by an angle equal to zero about the vertical axis [29]). The mechanism and the notation used to describe its configuration will be reviewed in Section II. The current design and the set of design parameters will also be introduced at this stage. Subsequently, numeric procedures for a combined enhancement of the workspace capabilities and kinematic performances of the mechanism will be presented in this paper. More specifically, this will be done by considering two possible commercial applications for the mechanism, each of them leading to a maximization of a particular 3-D subset of the 6-D complete workspace of the manipulator. Such an approach is consistent, as no method exists for the computation and graphical representation of the complete workspace of parallel manipulators.

1) *Design 1:* This statically balanced parallel mechanism could find great potential as a positioning and orienting device of heavy loads. In this context, we make the preliminary assumption that allowable rotational displacements of the pitch, yaw, and roll angles greater or equal to $\pm 20^\circ$ will be considered satisfactory for such an application. In addition, the translational DOFs of the mobile platform need to be maximized, ensuring simultaneously that the associated range of motion does not contain any singular configuration. Therefore, an optimization procedure for the maximization of the volume of the singularity-free region of the 3-D constant-orientation workspace of the parallel mechanism will be presented in Section III.
2) *Design 2:* The mechanism could also find great potential as a motion base for flight simulators. For such an application, it is well known that the motion of the cockpit does not require a large range of motion in the (x, y) plane and about the mobile z axis. It is, rather, necessary to maximize the rotational and translational displacements of the three remaining generalized coordinates, i.e., the rotational displacements associated with the roll and pitch angles, and the translational displacement along the z axis. We, therefore, make the preliminary assumption that, for the scale-down version of the mechanism considered, allowable translational displacements greater or equal to ± 80 mm in the x and y directions, and allowable rotational displacements greater or equal to $\pm 15^\circ$ about the mobile z axis will be considered satisfactory for such an application. As no method has been proposed in the literature for the computation and plotting of this 3-D workspace, a discretization method for the computation and graphical representation of this new workspace with coupled translational and rotational DOFs is proposed in Section IV. A second optimization procedure is then presented for the maximization of the volume of this second subset of the complete workspace. Our purpose here is to attempt a second optimal design of the mechanism by maximizing the volume of the associated 3-D Cartesian region that is also free of critical singularity loci.

Note that both optimization procedures are completely independent, and are used to improve the performances of this

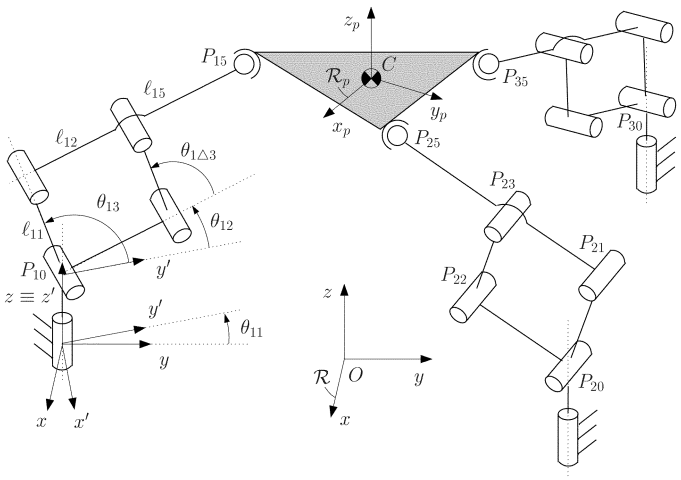

Fig. 2. Geometric parameters of the three-leg 6-DOF parallel manipulator.

three-leg statically balanced parallel mechanism with a view to two distinct future applications. The resulting sets of design characteristics will finally be discussed and compared in Section IV-E.

II. Existing Prototype and Choice of Optimization Parameters

A. Review of the Architecture

The type of mechanism considered in this paper is shown in Fig. 1. The architecture consists of a fixed base and a mobile platform connected by three legs. The ith leg is attached to the base at point P_{i0}, and to the mobile platform at point P_{i5} (see Fig. 2). In order to give symmetry to the architecture, the attachment points on the base and mobile platforms form equilateral triangles. We define a geometric parameter r that is used to describe the position of points P_{i0}, making the assumption that the attachment points of the three legs are equally spaced on a circle of radius r with center at point O, i.e., $r = \|\mathbf{p}_{i0}\|$, for $i = 1, 2, 3$. Starting from the base, the ith leg of the mechanism is a serial arrangement of a passive vertical revolute joint associated with angle θ_{i1}, a five-bar linkage located in the (y', z') plane, and a passive spherical joint connecting the leg to the mobile platform at point P_{i5}. The two proximal links of the five-bar linkage are mounted using two actuated revolute joints with coincident axes, associated, respectively, with angles θ_{i2} and θ_{i3}. The whole leg can rotate about the vertical z axis at point P_{i0}, that rotation including the mounting points of the springs at the base, so that the springs always remain in the plane of the five-bar linkage. The mobility $\mathfrak{M}$ of the parallel mechanism under study can be determined by application of the Chebyshev–Grübler–Kutzbach formula, i.e.,

$$\mathfrak{M} = 6(b - g - 1) + \sum_k f_k \tag{1}$$

where b and g are, respectively, the number of bodies (including the base) and number of joints of the mechanism, and f_k is the number of DOFs of joint k. Given the particular topological structure of the mechanism, and considering that each five-bar linkage is kinematically equivalent to a planar *RR* linkage, we have $b = 11, g = 12$, and $\sum_k f_k = 18$, the mobility of the mechanism thus being equal to six. Correspondingly, this 6-DOF mechanism is actuated by a set of six input angles, θ_{i2} and θ_{i3}, for i =1–3.

Definition of Terms

- θ_{ij} angles describing the configuration of the ith leg ($j = 1, 2, 3$);
- O origin of the fixed frame $\mathcal{R}$ located at equal distance from the three points P_{i0}, for $i = 1, 2, 3$;
- C centroid of the mobile platform;
- $\mathbf{p}$ vector connecting the origin O of the fixed frame $\mathcal{R}$ to the centroid C (position vector of the platform);
- $\mathbf{Q}$ rotation matrix representing the orientation of the platform and defined by Euler angles (ϕ, θ, ψ);
- $\mathbf{p}_{i0}$ vector connecting the origin of the fixed frame $\mathcal{R}$ to the attachment point P_{i0} of leg i at the base;
- $\mathbf{p}_{i5}$ vector connecting the origin of the fixed frame $\mathcal{R}$ to the attachment point P_{i5} of leg i at the platform;
- $\mathbf{b}_i$ vector from centroid C to the attachment point P_{i5} of the ith leg with respect to the mobile frame $\mathcal{R}_p$;
- b distance between point C and the attachment points P_{i5} of the ith leg to the mobile platform, i.e., $b = \|\mathbf{b}_i\|$, for $i = 1, 2, 3$;
- ℓ_{ir} length of the rth link of leg i, for $i = 1, 2, 3$ and $r = 1, 2, 5$.

We define a fixed-base reference frame $\mathcal{R}$ with its origin at point O, and with axes x, y, and z such that the base z axis coincides with the axis of symmetry of the mechanism. A mobile frame $\mathcal{R}_p$ is chosen fixed to the mobile platform at point C, with axes x_p, y_p, and z_p, such that the mobile z_p axis coincides with the axis of symmetry. In the *reference orientation* of the mobile platform, the orientation of the mobile frame coincides with that of the base frame. This orientation will be represented here by Euler angles ϕ, θ, and ψ. Note that different conventions for the Euler angles will be used in this paper in correspondence with the particular 3-D subset of the complete workpsace to be computed. The set of Euler angles and the corresponding rotation matrices will be described in Sections III and IV, respectively. The position of the mobile platform is described by the vector $\mathbf{p} = [x, y, z]^T$, which denotes the coordinates of the point C and expressed in the reference frame $\mathcal{R}$. In this context, $(x, y, z, \phi, \theta, \psi)$ denote the generalized coordinates of the manipulator. The reader should refer to Fig. 2 and to the associated definition of terms for a description of the mechanism and its configuration.

B. Balancing Conditions and Corresponding Choice of Optimization Parameters

As mentioned previously, the geometric characteristics of the prototype shown in Fig. 1 led to an architecture which may not be optimal from a kinematic perspective. This motivated the implementation of optimization procedures for the improvement of the workspace capabilities and kinematic performances of the mechanism. However, this optimization problem cannot be addressed using a procedure similar to what can be implemented

for conventional nonbalanced spatial parallel manipulators. Indeed, the design of such a statically balanced manipulator imposes that the optimization of the kinematic parameters of the mechanism be determined through a two-step approach.

Glossary of Static Balancing-Related Parameters

- k_{ij} stiffness of the jth spring of leg i;
- h_{ij} distance from point P_{i0} to the mounting point of the jth spring of leg i to the base;
- σ_{ij} fixed angle between the vertical axis and the line passing through point P_{i0} and the mounting point of the jth spring of leg i to the base;
- s_{ij} distance from point P_{i0} to the extremity of the jth elongated link of the parallelogram;
- m_p fixed mass of the mobile platform + payload;
- m_{ir} mass of the rth link of leg j;
- $\mathbf{c}_p$ position vector of the center of mass of the mobile platform and expressed in mobile frame $\mathcal{R}_p$;
- $\mathbf{c}_{ir}$ position vector of the center of mass of the rth link of leg j expressed in a local frame.

First, the subset of kinematic parameters that appear in the balancing conditions must be determined in order that the total potential energy of the system be constant for any configuration, i.e., the coefficients of the configuration-dependent terms in the expression of the potential energy be equal to zero. This first phase of the design process was completely addressed in [10] and [17] for the class of mechanism considered in this paper. A set of sufficient balancing conditions was obtained in the form of a complex system of 13 nonlinear algebraic equations, i.e.,

$$\mathbf{f}(m_p,\mathbf{c}_p,\mathbf{b}_i,m_{ir},\mathbf{c}_{ir},\ell_{ir},k_{ij},h_{ij},s_{ij},\alpha_{ij})=\mathbf{0},\quad i=1,2,3,\quad j=2,3,\quad r=1,2,5 \tag{2}$$

where $\mathbf{0}$ is the (13×1) zero vector. The additional scalar and vector variables appearing in (2) are defined in the glossary of terms associated with Fig. 3.

Among the design variables appearing in (2) that were computed during the first stage of the design process, only the lengths $\ell_{ir}, i=1,2,3, r=1,2,5$ of the links of the legs and the components of vectors $\mathbf{b}_i, i=1,2,3$ affect the workspace shape and the location of the singularities of the mechanism. As these parameters were determined in order that the static balancing of the mechanism be accomplished, they are considered as constant input data (their values are given in Table II). Hence, the integrity of the balancing conditions will be preserved during the subsequent optimization procedures.

Then, we have to determine the maximum subset of remaining kinematic parameters that do not affect the balancing conditions. These parameters will be used as optimization parameters to improve the workspace and kinematic properties of the mechanism. Subsequently, the balancing conditions do not depend on the location of the attachment points $P_{i0}, i=1,2,3$ of the legs to the base. Having made the assumption that these points are located on a circle of radius r with center at point O, the distance r can be regarded as a first optimization parameter. In addition, let (δ_i) be the axis of symmetry of the cone of mobility of the spherical joint attached to the ith leg (see Fig. 3).

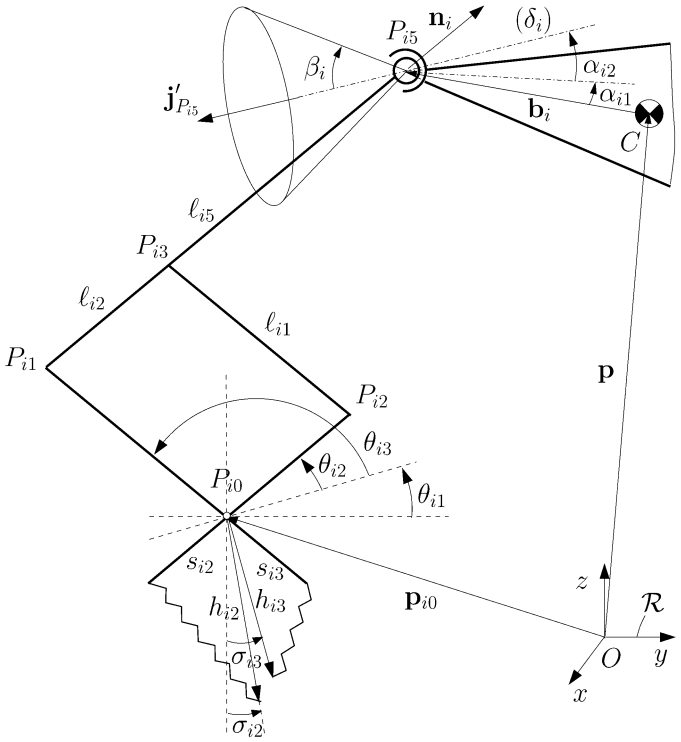

Fig. 3. Design parameters associated with leg i.

The orientation of the (δ_i) axis with respect to the mobile frame, represented by angles α_{i1} and α_{i2}, do not affect the balancing conditions either. In this orientation representation, angle α_{i2} is the angle beetween the axis (δ_i) and the projection of this axis onto the mobile (x_p, y_p) plane. The projection of axis (δ_i) then makes an angle α_{i1} with the vector $(-\mathbf{b}_i)$. As for most commercial applications of parallel manipulators, it is desirable to achieve a symmetric design for the mechanism. We, therefore, impose the nonrestrictive additional conditions $\alpha_{11}=\alpha_{21}=\alpha_{31}=\alpha_1$ and $\alpha_{12}=\alpha_{22}=\alpha_{32}=\alpha_2$. Our set of optimization parameters is finally described by the vector (α_1,α_2,r).

III. First Optimization Procedure Based on the Constant-Orientation Workspace

In this section, we consider a first application of the mechanism as a positioning and orienting device of heavy loads. In this context, we present a procedure for the maximization of the volume of the 3-D region of the constant-orientation workspace that is free of critical singularities. Several methods are currently available in the literature for the computation of the constant-orientation workspace of parallel manipulators (see, for instance, [26] for a detailed classification of these methods). Representative of the first class of methods are the purely geometrical approaches proposed in [13] and [15], and extended in [26] to account for the mechanical constraints associated with the range of motion of the passive joints and the leg interferences.

The second class of methods are referred to as *discretization techniques* (e.g., [1], [8], and [25]). In the most basic ones, a sufficient large cubic region from the Cartesian space is completely discretized. Then, for each node of this cubic grid, the inverse kinematics is solved, and a set of mechanical constraints is

tested. In probably the most sophisticated and fastest discretization method, the boundary of the workspace is determined in a spherical coordinate system by discretizing the range of azimuth and zenith angles [8]. Despite such methods are computationally intensive and give little information about the geometric nature of the workspace boundary, they can be easily applied to any type of parallel manipulator for virtually any set of mechanical constraints. In addition to all conventional mechanical limits, it is intended here to incorporate the closed-form equations for the singularity loci of the three-leg 6-DOF parallel mechanism in the set of kinematic constraints. For inherent complexity reasons, the discretization algorithm proposed in [8] was found to be the most appropriate candidate to be used in the following design procedure.

A. Conventional Mechanical Constraints

This section summarizes the conventional mechanical constraints that limit the constant-orientation workspace of the mechanism. As a preliminary, let us be precise that the orientation of the platform will be represented in this section by the ZXY Euler-angle convention that is defined by first rotating the mobile frame about the base z axis by an angle ϕ, then about the new x axis by an angle θ, and finally about the mobile y_p axis by an angle ψ. For this choice of Euler angles, the singularity occurs at $\theta = \pm\pi/2$ and the rotation matrix is defined as

$$\begin{aligned}\mathbf{Q} &= \mathbf{Q}_z(\phi)\mathbf{Q}_x(\theta)\mathbf{Q}_y(\psi) \\ &= \begin{bmatrix} (c_\phi c_\psi - s_\phi s_\theta s_\psi) & -s_\phi c_\theta & (c_\phi s_\psi + s_\phi s_\theta c_\psi) \\ (s_\phi c_\psi + c_\phi s_\theta s_\psi) & c_\phi c_\theta & (s_\phi s_\psi - c_\phi s_\theta c_\psi) \\ -c_\theta s_\psi & s_\theta & c_\theta c_\psi \end{bmatrix} \end{aligned} \quad (3)$$

where $c_\phi \equiv \cos\phi, s_\phi \equiv \sin\phi, c_\theta \equiv \cos\theta$, etc.

Subsequently, there exists four main sets of basic mechanical constraints that limit the constant-orientation workspace of the three-leg parallel mechanism, viz.: 1) the limited length of the legs; 2) the range of motion of the three spherical joints; 3) the leg interferences; and 4) additional constraints related to the mechanical design.

1) Limited Length of the Legs: Let the orientation of the mobile platform be represented by the (3×3) orthogonal rotation matrix $\mathbf{Q}$. For a given position (vector $\mathbf{p}$) and orientation (matrix $\mathbf{Q}$) of the mobile platform, the necessary leg lengths, denoted by M_i, are computed using the following relation, $i = 1, 2, 3$:

$$M_i = \|\mathbf{p}_{i5} - \mathbf{p}_{i0}\| = \|\mathbf{p} + \mathbf{Q}\mathbf{b}_i - \mathbf{p}_{i0}\|. \quad (4)$$

Then, the five-bar linkage structure of the legs imposes a length constraint such that

$$\ell_{i5} - \ell_{i2} + \xi_{i1} \le M_i \le \ell_{i5} + \ell_{i1} - \xi_{i2} \quad (5)$$

where ℓ_{i1}, ℓ_{i2}, and ℓ_{i5} are, respectively, the lengths of the elements of leg i (see Fig. 2), and ξ_{i1} and ξ_{i2} are constant terms used to account for the range of reachable positions by each parallelogram structure.

2) Range of Motion of the Spherical Joints: Let $\mathbf{j}'_{P_{i5}}$ be the unit vector collinear with the axis (δ_i) and expressed in the mobile frame $\mathcal{R}_p$ (see Fig. 3). Let vector $\mathbf{j}_{P_{i5}}$ be the opposite vector, and with respect to the base frame, i.e., $\mathbf{j}_{P_{i5}} = -\mathbf{Q}\mathbf{j}'_{P_{i5}}$. Let the maximum misalignment angle of that joint be β_i. Then, the limits on the mobile platform joint i impose an angular constraint such that, for $i = 1, 2, 3$

$$\cos^{-1}\left((\mathbf{j}_{P_{i5}})^T \mathbf{n}_i\right) \le \beta_i \quad (6)$$

where unit vectors $\mathbf{n}_i = (\mathbf{p}_{i5} - \mathbf{p}_{i1})/\ell_{i5}$ are defined as

$$\mathbf{n}_i = \begin{bmatrix} \cos\theta_{i1} & -\sin\theta_{i1} & 0 \\ \sin\theta_{i1} & \cos\theta_{i1} & 0 \\ 0 & 0 & 1 \end{bmatrix} \begin{bmatrix} 0 \\ \cos\theta_{i2} \\ \sin\theta_{i2} \end{bmatrix}, \quad i = 1, 2, 3 \quad (7)$$

and unit vectors $\mathbf{j}'_{P_i5}, i = 1, 2, 3$ are given by

$$\begin{aligned}&\left[\mathbf{j}'_{P_15}, \quad \mathbf{j}'_{P_25}, \quad \mathbf{j}'_{P_35}\right] \\ &= \left[\begin{array}{c|c|c} c_{\alpha_2}c_{(\alpha_1+\pi/3)} & c_{\alpha_2}s_{(\alpha_1+\pi/6)} & -c_{\alpha_2}c_{\alpha_1} \\ -c_{\alpha_2}s_{(\alpha_1+\pi/3)} & c_{\alpha_2}c_{(\alpha_1+\pi/6)} & -c_{\alpha_2}s_{\alpha_1} \\ -s_{\alpha_2} & -s_{\alpha_2} & -s_{\alpha_2} \end{array}\right] \end{aligned} \quad (8)$$

where $c_{\alpha_2} \equiv \cos\alpha_2, c_{(\alpha_1+\pi/3)} \equiv \cos(\alpha_1 + \pi/3)$, etc.

3) Leg Interferences: Let us make the assumption that the elements of the three legs can be approximated by cylinders of diameter D. We point out that, for most configurations of the mobile platform, only strut collisions between segments $P_{i2}P_{i3}$ and $P_{i3}P_{i5}$ of leg i with segment $P_{j1}P_{j5}$ of leg $j, i \neq j$ are a concern. Thus, the structure of the three-leg mechanism using five-bar linkages imposes a set of constraints, such that

$$\begin{cases} \text{distance}\,(P_{i2}P_{i3}, P_{j1}P_{j5}), & \ge D \\ \text{distance}\,(P_{i3}P_{i5}, P_{j1}P_{j5}), & \ge D \\ i, j = 1, 2, 3, \quad i \neq j. \end{cases} \quad (9)$$

These contraint check equations require the computation of the minimum distance between two line segments, which requires the implementation of a multistep algorithm. We do not recall such an algorithm here due to space limitations, but we refer the reader to the one presented in [25].

4) Additional Constraints: The specific design of the base platform of the prototype imposes to consider the following constraint:

$$z > 0. \quad (10)$$

B. Singularity Loci and Inherent Kinematic Constraints

In this section, the singularity loci of the three-leg parallel mechanism are summarized and their constitutive equations are given in closed form to be incorporated as kinematic constraints in the following discretization algorithms. The singularities of the mechanism were determined in [29] using Grassmann line geometry. Five families of singularities were identified.

1) The two links of the ith leg are aligned, i.e., $\sin\triangle\theta_{i3} = 0$. This defines, for each leg i, the minimum and maximum spheres of radii $(\ell_{i5} - \ell_{i2})$ and $(\ell_{i5} + \ell_{i1})$, respectively, with center at point of coordinates $(\mathbf{p}_{i0} - \mathbf{Q}\mathbf{b}_i)$, that constitute the boundary of the constant-orientation workspace of the mechanism. The constraint expressed by (5) takes already care of this case.
2) When the mobile and base platforms are parallel, i.e., $\theta = \psi = 0$, a singularity occurs when the angle of rotation ϕ of the platform about the z axis is equal to 0 or π.

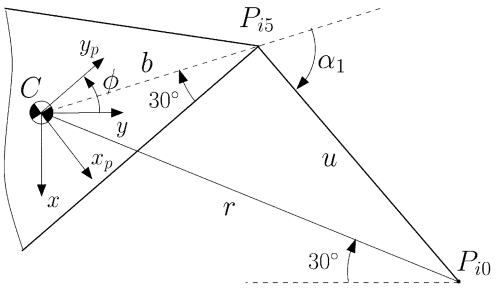

Fig. 4. Leg i of the mechanism (top view).

3) In the case of an arbitrary orientation of the mobile platform, a singular configuration occurs when the end-effector is located on a quadratic surface represented in the Cartesian space by

$$E_1x^2 + E_2y^2 + E_3xy + E_4x + E_5y + E_6 = 0 \qquad (11)$$

which correspond to either a hyperbolic, a parabolic, or an elliptic cylinder, oriented along the z axis. Coefficients $E_i = E_i(\phi, \theta, \psi, r, b), i = 1, \ldots, 6$, are given in [29]. The criticality of such singularities was shown in that reference.

4) A singularity occurs when the platform is purely rotated by $\pm\pi/2$ about a median of triangle $P_{15}P_{25}P_{35}$. Such singularities will always be located far outside the workspace boundary and will, therefore, be neglected here.

5) Additional singular configurations occur when the upper end of leg i, P_{i5} is exactly above its lower end, P_{i0}, for $i = 1, 2, 3$. The corresponding singularity loci are three vertical lines that pass through the point of coordinates $(\mathbf{p}_{i0} - \mathbf{Q}\mathbf{b}_i), i = 1, 2, 3$. In practice, these lines can easily be avoided during any trajectory tracking and will, therefore, be neglected in the discretization procedure.

As it was found numerically that the left-hand expression in (11) is strictly positive inside the region that is free of such singularities, it was finally decided to incorporate the following set of kinematic constraints:

$$0 < \phi < \pi \qquad (12)$$

$$E_1x^2 + E_2y^2 + E_3xy + E_4x + E_5y + E_6 > 0. \qquad (13)$$

C. Workspace Volume Optimization Algorithm

1) Preliminary Calculations: The consistency of the optimization process imposes that the angle between the leg and the axis of symmetry of the spherical joints, projected onto the (x, y) plane, be equal to zero when the mobile platform is in the configuration $(x, y) = (0, 0)$. This ensures that the workspace is computed with a starting appropriate neutral orientation of the mobile platform about the vertical axis. In this context, a constant average value of angle ϕ, noted ϕ_{av}, is computed for each value of parameter α_1 (see Fig. 4). Let u be the projected distance between the two attachment points of the ith leg P_{i0} and P_{i5}. For a given value of angle α_1, the angle ϕ_{av} is readily determined by the set of equations

$$r^2 = b^2 + u^2 + 2bu\cos\alpha_1 \qquad (14)$$

$$u^2 = r^2 + b^2 - 2br\cos\phi_{\text{av}} \qquad (15)$$

which leads to the following quadratic equation in $\cos\phi_{\text{av}}$:

$$A(\cos\phi_{\text{av}})^2 + B\cos\phi_{\text{av}} + C = 0 \qquad (16)$$

with

$$\begin{cases} A = r^2 \\ B = 2br(\cos^2\alpha_1 - 1) \\ C = b^2(1 - \cos^2\alpha_1) - r^2\cos^2\alpha_1. \end{cases} \qquad (17)$$

As we only consider the positive values of angle ϕ, (16) results in two solutions. Then, it can be shown that the structure of the three-leg mechanism imposes that only the smallest of the remaining solutions has to be considered.

2) Review of the Discretization Technique for the Computation of the Constant-Orientation Workspace: The discretization technique presented in [8] is based on the integrated implementation of the following two algorithms.

Spherical Search Algorithm: Let us assume that the location of an approximated center O_c of the workspace is known for a given orientation of the platform. This algorithm then conducts a search to determine the boundary of the workspace in a spherical coordinate system $(\rho_c, \eta_c, \gamma_c)$ with center at point O_c. The process of searching the entire space is accomplished by discretizing the range of azimuth and zenith angles η_c and γ_c. For each pair of them, the radius ρ_c is incremented until a constraint violation is detected. When a value for ρ_c is found to be located outside the workspace, which constitutes a first approximation for the location of the workspace boundary along the spherical ray, a second algorithm, referred to as the *Workspace Boundary Algorithm*, is used to refine the result.

Workspace Boundary Algorithm: For each pair of azimuth and zenith angles, this algorithm is used at the final stage of the search process. It is based on the use of an *interval-halving* search technique in order to guarantee that ρ_c is within $\pm\varepsilon$ of the workspace boundary, where ε is a given error tolerance.

The consistency and accuracy of the method are demonstrated in [8] using various examples. We now present the algorithm for the maximization of the volume of the 3-D region of the constant-orientation workspace of the three-leg mechanism that is free of critical singularity loci. The procedure is described schematically in Fig. 5.

3) Algorithm for the Maximization of the Volume of the Singularity-Free Region of the Constant-Orientation Workspace:

S1. Initialize 3-D array $\mathbf{V}_1$ with dimensions $(n_{\alpha_1} \times n_{\alpha_2} \times n_r)$, where $n_{\alpha_1}, n_{\alpha_2}$, and n_r are, respectively, the number of incremental steps corresponding to α_1, α_2, and r.

S2. Start with initial values of optimization parameters $\alpha_1 = \alpha_{1,\min}, \alpha_2 = \alpha_{2,\min}$, and $r = r_{\min}$.

S3. For the current set (α_1, α_2, r), do:

S4. Define a cube-shaped grid whose equally-spaced nodes describe positions of the mobile platform within the work volume of the mechanism. For each node of the grid whose position $\mathbf{p}$ and orientation $\mathbf{Q}$ is known, angles $\theta_{ij}, i = 1, 2, 3, j = 2, 3$ are computed using the expressions for the inverse kinematics [9]. Then, (5), (6), (9), (10), (12), and (13) are employed to check for any constraint violation. Using the results obtained from testing these positions, the approximate location

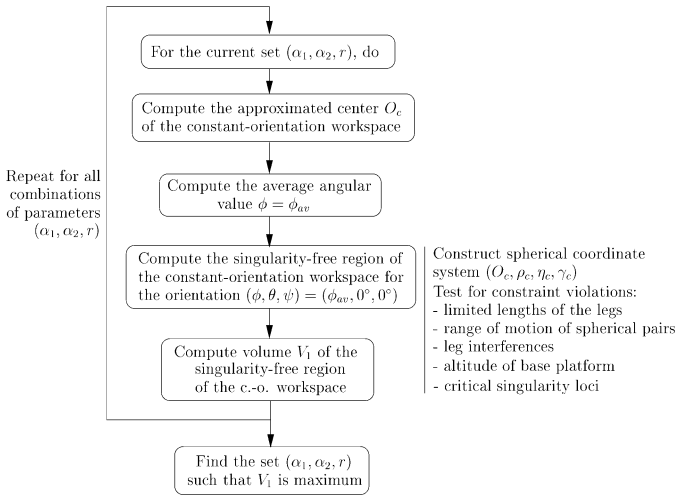

Fig. 5. Flowchart describing the first optimization procedure presented in Section III-C.3.

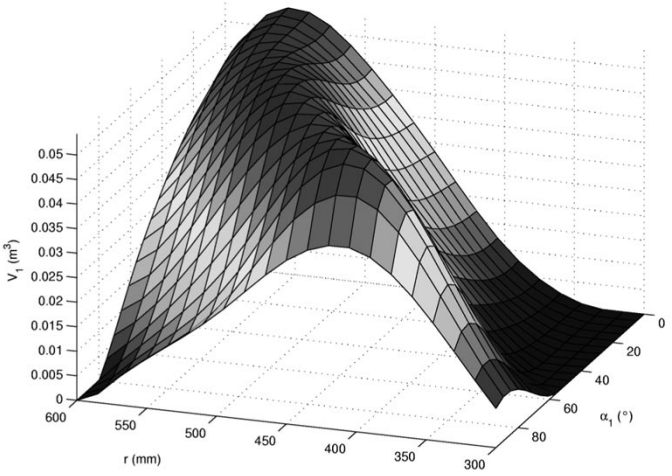

Fig. 6. Volume V_1 as a function of parameters α_1 and $r(\alpha_2 = 0°)$.

of the center O_c of the workspace can be determined. This center will serve as the origin of a spherical coordinate system $(\rho_c, \eta_c, \gamma_c)$.

S5. Initialize matrix $\mathbf{W}_\rho$ with dimensions $(n_{\eta_c} \times n_{\gamma_c})$, where n_{γ_c} and n_{η_c} define the number of incremental steps that constitute the spherical grid for $\gamma_c = 0°, \ldots, 180°$ and $\eta_c = 0°, \ldots, 360°$.

S6. Solve (16) to compute the corresponding average angular value $\phi = \phi_{\text{av}}$.

S7. Use the *Spherical Search Algorithm* and the *Workspace Boundary Algorithm* presented in [8] to compute the corresponding region of the constant-orientation workspace that is free of critical singularities in spherical coordinates for the orientation $(\phi, \theta, \psi) = (\phi_{\text{av}}, 0°, 0°)$. For each node of the spherical grid, the inverse kinematic problem is solved, and the constraint violations are detected by (5), (6), (9), (10), (12), and (13). The values of radius ρ_c at the points of constraint violation are stored into matrix $\mathbf{W}_\rho$.

S8. Each sector of the resulting workspace being approximated by a four-sided pyramid defined by four adjacent workspace data point $\mathbf{W}_\rho[i, j]$ with origin at point O_c, determine the volume of the workspace by summing the calculated volumes of all the sectors. The value of the workspace volume is then stored in the 3-D array $\mathbf{V}_1$.

S9. Repeat steps S3–S8 for all possible combinations of optimization parameters (α_1, α_2, r).

S10. Plot resulting data to find the set of parameters (α_1, α_2, r) which corresponds to a maximal volume of the singularity-free workspace of the three-leg mechanism.

4) Results: The algorithm was developed in MATLAB code for its convenience in manipulating multidimensional arrays and for its wide range of visualization capabilities. In our implementation, we use the data given in the Appendix, with a number of incremental steps $n_{\phi_c} = 91, n_{\theta_c} = 61, \varepsilon = 1$ mm, and with generalized coordinates $\theta = \psi = 0°$. The choice of discretization intervals of 4° and 3° for the azimuth and zenith angles resulted from a compromise between the computational time required to compute the workspace and the accuracy when computing its associated volume. As parameter design is an offline process, we could deal with large computational times and choose small intervals. The choice of such values for the discretization intervals ensured that the error between the actual volume of the workspace and the computed one remained inferior to 0.1%. Then, in order to facilitate the graphical interpretation of the results, it was decided to plot the different surfaces defined by

$$V_1 = f_{\alpha_2}(\alpha_1, r), \quad \alpha_2 \in [\alpha_{2,\min}, \alpha_{2,\max}]. \tag{18}$$

This study allows making the two following observations.

1) The resulting surfaces, similar to the one given in Fig. 6, all contain a continuum of local extrema. Variations of angle α_2 do not affect the global nature of the surface but have an impact on the location of these extrema.
2) For $\alpha_2 = 0°$, we point out that the corresponding range of local extrema contains all possible maximal values of the volume V_1 of the workspace, $(\forall\ \{\alpha_1, r\})$.

For the manipulator under study, these properties allow choosing an arbitrary value of α_1 such that $\alpha_1 \in]0°, 80°]$, for which we can then always find a corresponding value of r such that the volume of the workspace represents at least 97% of its maximum value (see Fig. 6). Considering that the motion of the mechanism is limited to the half-complete workspace defined by $\phi > 0$, the axis of symmetry of the cone of mobility of the spherical joint attached to the ith leg has to be designed such that $\alpha_1 > \beta_i, i = 1, 2, 3$. This allows maximizing the amount of possible rotations around the z axis. Given that $\beta_i = 35°$, for $i = 1, 2, 3$, we point out that a relevant compromise is to choose $\alpha_1 = 45°$. This finally leads to a particular set of geometric parameters, such that $r = 504$ mm, i.e., $r = 2.4b, \alpha_1 = 45°(\phi_{\text{av}} = 28°)$, and $\alpha_2 = 0°$ (see Fig. 6). The corresponding maximum volume of the workspace is equal to 0.055 m^3. This volume is three times larger than the equivalent one computed for the initial version of the mechanism shown in Fig. 1. The resulting constant-orientation workspace, on which a cross section in the (x, y) plane of

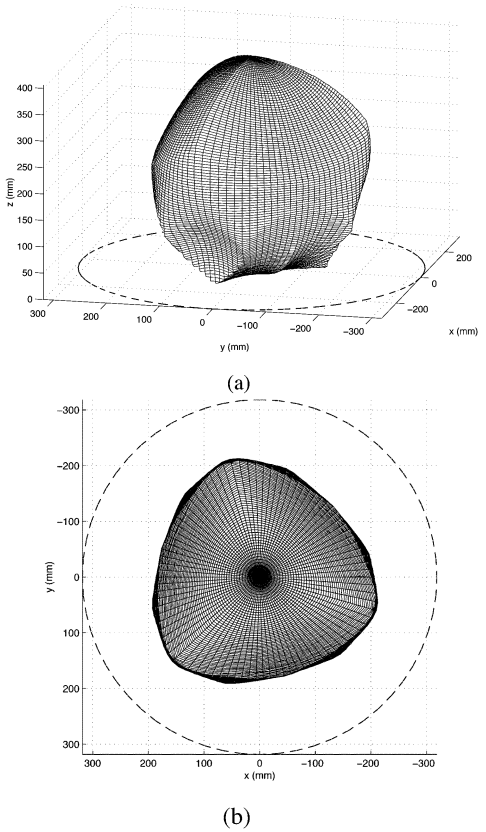

Fig. 7. (a) Perspective and (b) top views of the maximal singularity-free constant-orientation workspace of the mechanism $(\alpha_1, \alpha_2, r) = (45°, 0°, 504)$ mm, $(\phi, \theta, \psi) = (28°, 0°, 0°)$.

the singularity surface given by (13) is superimposed (dashed circle), is represented in Fig. 7. Note, correspondingly, that the optimized workspace is much smaller that the 3-D region free of singularities, i.e., the constraint violation expressed by (13) was never encountered for this set of design parameters. In that case, the region of the workspace that is free of singularities is constituted by the whole workspace. In fact, it was observed during the optimization process that, when the singularity surface is tangent to the boundary of the workspace, the radius of the cylinder of singularities and the corresponding volume of the singularity-free workspace are much smaller than those for the optimum case. Such a result is all the more interesting as it means that the Jacobian matrix of the mechanism will be well conditioned throughout and even near the boundary of the workspace. The design characteristics for this first optimization are summarized in Table I.

Note: The optimization procedure was implemented for the case where $\theta = \psi = 0°$, which could appear restrictive from a design perspective. However, allowable rotational displacements of the pitch, yaw, and roll angles greater than $\pm 20°$ were obtained, i.e., $\triangle\phi = \pm 30°$ and $\triangle\theta = \triangle\psi = \pm 25°$, thus exceeding the desired ranges of possible rotations of the mobile platform as provided in Section I for a commercial application of the mechanism as a positioning and orientating device of heavy loads. Let us mention that, if rotational displacements inferior to $\pm 20°$ had been obtained, an alternative approach consisted in the determination of

TABLE I
GEOMETRIC DATA BEFORE/AFTER OPTIMIZATION ($\triangle q$ DENOTES MAXIMUM ALLOWABLE DISPLACEMENT FOR COORDINATE q, AND ROTATIONS ARE REPRESENTED BY ZXY EULER ANGLES)

Geometric data	Initial prototype	Optimized design 1	Optimized design 2
r in [mm]	280	504	280
α_1 in [°]	0	45	85
α_2 in [°]	45	0	30
V_1 in $[\mathrm{m}^3]$	0.019	0.055	0.037
V_2 in $[\mathrm{m}\cdot\mathrm{rad}^2]$	0.186	0.119	0.245
$\triangle x$ in [mm]	± 60	± 180	± 109
$\triangle y$ in [mm]	± 60	± 180	± 109
$\triangle z$ in [mm]	± 176	± 190	± 220
$\triangle\phi$ in [°]	± 8	± 30	± 25
$\triangle\theta$ in [°]	± 28	± 25	± 33
$\triangle\psi$ in [°]	± 28	± 25	± 33

the optimum set (α_1, α_2, r) such that the average volume $\overline{V}_1 = 1/(n_\theta n_\psi) \sum_{\triangle\theta} \sum_{\triangle\psi} V_1(\phi_{\mathrm{av}}, \theta, \psi)$ be maximum, where $\triangle\theta = \triangle\psi = \pm 20°$, and n_θ and n_ψ are the number of discrete intervals over $\triangle\theta$ and $\triangle\psi$, respectively.

It should finally be highlighted that, for the three-leg mechanism, neglecting the mechanical constraint associated with the range of motion of the spherical joints would have led to a maximal volume equal to 0.085 m^3 for the geometry $\alpha_1 = 58°$ and $r = 2.2b$. Thus, neglecting these mechanical constraints can introduce significant errors and lead to a feasible but nonoptimal design.

IV. SECOND OPTIMIZATION PROCEDURE BASED ON A NEW WORKSPACE WITH COUPLED TRANSLATIONAL AND ROTATIONAL GENERALIZED COORDINATES

In this section, we consider a second application of the mechanism as a motion base for flight simulators. As discussed in Section I, we present a procedure for the maximization of the volume of the 3-D workspace with constant translational x and y coordinates and constant rotation angle of the platform about the mobile z_p axis. Our purpose is to attempt a second optimal design of the mechanism by maximizing the volume of the associated 3-D Cartesian region that is also free of critical singularity loci. As no method has been proposed in the literature for the computation and plotting of this workspace, a discretization method for the computation and graphical representation of this new workspace with coupled translational and rotational DOFs is proposed in this section. Note, correspondingly, that the computation of this workspace is also of great interest in the context of analysis and design of new motion simulators with only three or four DOFs, currently developed for their lower manufacturing cost and simplified control algorithms.

A. Representation of the Platform Orientation

One of the major issues associated with the computation and graphical representation of such a workspace is the choice of the set of Euler angles to describe the orientation of the mobile platform. Various sets of Euler angles (ϕ, θ, ψ) exist, but

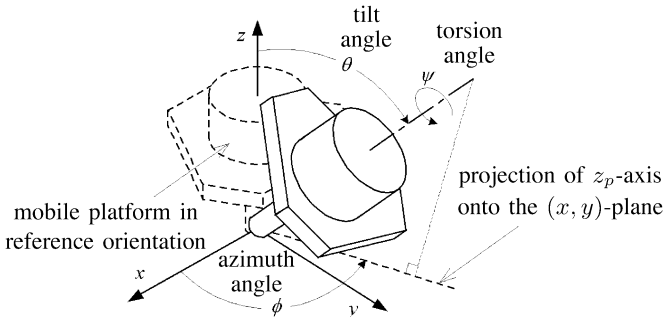

Fig. 8. Representation of the platform orientation using the tilt-and-torsion angles [4] (figure courtesy of Dr. I. A. Bonev).

their interpretation is generally nonintuitive. Let us recall that our purpose is to compute the 3-D workspace for the case when the rotation angle ψ of the platform about the mobile z_p axis, referred here to as the *torsion angle*, and the x and y coordinates of a reference point of the platform, are prescribed. Hence, we impose the first requirement that Euler angles ϕ and θ must describe exactly the direction of the z_p axis with respect to the fixed frame $\mathcal{R}$. Moreover, we impose the second requirement that Euler angles ϕ and θ must correspond to the azimuth and zenith angles that define the direction of the z_p axis in a spherical coordinate system, thus ensuring a easy and intuitive interpretation of the platform orientation. These requirements are adequately met by the *tilt-and-torsion* angles (see Fig. 8). This orientation parametrization was introduced in [3] for the computation of the orientation workspace of parallel manipulators, defined as the set of all attainable orientations of the platform about a point being fixed with respect to the base frame, and later applied to the analysis of constrained manipulators in [4]. This modified set of Euler angles was also used in [20] for representing the 2-D orientation workspace of Gough–Stewart parallel manipulators. In this orientation representation, the mobile platform is first rotated about the base z axis by an angle ϕ, then about the new y axis by an angle θ, and finally about the mobile z_p axis by an angle $\psi - \phi$. The singularity occurs at $\theta = 0°$, and the corresponding rotation matrix is given by

$$\mathbf{Q} = \mathbf{Q}_z(\phi)\mathbf{Q}_y(\theta)\mathbf{Q}_z(\psi-\phi) = \begin{bmatrix} c_\phi c_\theta c_{(\psi-\phi)} - s_\phi s_{(\psi-\phi)} & -c_\phi c_\theta s_{(\psi-\phi)} - s_\phi c_{(\psi-\phi)} & c_\phi s_\theta \\ s_\phi c_\theta c_{(\psi-\phi)} + c_\phi s_{(\psi-\phi)} & -s_\phi c_\theta s_{(\psi-\phi)} + c_\phi c_{(\psi-\phi)} & s_\phi s_\theta \\ -s_\theta c_{(\psi-\phi)} & s_\theta s_{(\psi-\phi)} & c_\theta \end{bmatrix}. \quad (19)$$

A one-to-one correspondence exists between the orientations of the mobile platform and the orientation parametrization used when angles ϕ, θ, and ψ are defined over the intervals $]-180°, 180°]$, $[0°, 180°]$, and $]-180°, 180°]$, respectively. As we will see in Section IV-C, this particular orientation parametrization allows the representation of the workspace with x, y, and ψ constant as a single volume with a compact shape.

B. Represention of the Workspace

It was chosen to represent the workspace with coupled translational/rotational DOFs in a cylindrical coordinate system, where ϕ and θ are the polar angles and z is exactly the z coordinate, for two main reasons. First, for each plane defined by $z = \text{const}$, the process of searching the workspace boundary always starts from an approximated neutral configuration, and the workspace is, therefore, not delimited by an inner boundary. This ensures a representation of the workspace as a single volume whose boundary is always visible and easy to interpret. Secondly, for each plane $z = \text{const}$, all possible orientations will be attainable from the approximated neutral configuration through a continuous motion without violating any mechanical constraint, thus avoiding the issue related to the *compatibility constraint*, as reported in [3].

We now present the discretization algorithm for the computation of the workspace with coordinates x, y, and ψ constant. This algorithm is a modified version of the one that was first introduced in [3] to compute the orientation workspace, in which angle ψ is substituted by coordinate z. It is intrinsically applicable to any type of spatial parallel manipulator with the aforementioned DOFs of the platform, for any set of mechanical constraints. Let x_c, y_c, and ψ_c be the constant values for x, y, and ψ. Finally, let z_f be the z coordinate of a point that is located above the top of the workspace, the algorithm is then as follows.

C. Discretization Algorithm for the Workspace With Coupled Translational/Rotational DOFs

S1. Set $\psi = \psi_c, x = x_c, y = y_c$. Define a linear grid along the z axis whose equally spaced nodes describe positions of the platform within the work volume of the mechanism. Then, solve the inverse kinematics and apply the set of constraint checks for each node of the grid. Using the results obtained from testing these positions, the approximate z coordinate z_c of the workspace center can be determined.

S2. Set $z = z_c$. Assume that $(\phi_c, \theta_c) = (0°, 0°)$ is the center of the horizontal cross section of the workspace for $z = z_c$.

S3. Initialize matrices $\mathbf{W}_{\phi,u}$ and $\mathbf{W}_{\theta,u}$, with dimensions $(n_z/2+1)\times n_\phi$, where n_z+1 is the number of equally spaced planes $z = \text{const}$ between $z = 0$ and $z = z_f$ at which the workspace will be computed, and n_ϕ is the number of discrete points to be computed at each plane $z = \text{const}$. These matrices will store, respectively, the values of ϕ and θ for the points defining the upper part of the workspace.

S4. For the current z, construct a polar coordinate system at (ϕ_c, θ_c). Starting at n_ϕ equally spaced angles, increment the polar ray, solve the inverse kinematics, and apply the set of constraint checks until a constraint is violated. The values for ϕ and θ at the points of constraint violation are stored into the two matrices $\mathbf{W}_{\phi,u}$ and $\mathbf{W}_{\theta,u}$.

S5. Compute the geometric center (ϕ_c, θ_c) of the workspace cross section, which will serve as the assumed center for the next cross section. Set $z = z + z_f/n_z$.

S6. Perform steps S4 and S5 until the workspace cross section is a single point (i.e., $z_{\max}$ is reached).

S7. Assign to (ϕ_c, θ_c) the values that were stored in step S5 for $z = z_c$. Set $z = z_c - z_f/n_z$.

S8. Perform steps S3–S6 in a similar way with decreasing z coordinates to determine the lower part of the workspace. The points defining the lower part of the workspace are stored into matrices $\mathbf{W}_{\phi,l}$ and $\mathbf{W}_{\theta,l}$.

D. Workspace Volume Optimization Procedure

The algorithm presented in Section IV-C will be the core of a second optimization procedure for the maximization of the volume of the singularity-free workspace with x, y, and ψ constant of the three-leg mechanism shown in Fig. 1.

1) Modified Set of Constraints: In the following optimization algorithm, all conventional mechanical constraints defined by (5), (6), (9), and (10) will still be considered. However, the particular representation of the workspace with x, y, and ψ constant imposes that the kinematic constraints associated with the critical singularity loci reviewed in Section III-B to be reformulated. As a first iteration of the optimization algorithm will be run for the case $(x_c, y_c) = (0\text{ mm}, 0\text{ mm})$, which will be shown in Section IV-E to be sufficient to obtain very satisfactory results, (11), describing the critical singularity loci, will be readily rewritten under the form

$$E_6(\phi, \theta, \psi, r, b) = 0. \tag{20}$$

Then, we substitute the tilt-and-torsion angles in (20) and we perform the tangent-half substitution

$$\sin\theta = \frac{2U}{1+U^2}, \quad \cos\theta = \frac{1-U^2}{1+U^2} \tag{21}$$

with $U = \tan(\theta/2)$. After factorization, multiplication by $(1+U^2)$, and rearranging, (20) reduces to the form

$$\sin\psi[U^2(r + b\sin\psi\sin 2\phi + b\cos\psi\cos 2\phi) + r - b\cos\psi] \cdot[U^2(r^2 - b^2) + r^2 + b^2 - 2br\cos\psi] = 0. \tag{22}$$

The corresponding singularity loci are independent from the z coordinate and are, therefore, identical, whatever the cross section at $z = \text{const}$ of the workspace with x, y, and ψ constant to be considered. Then, the orientation representation imposes that we compute only positive values for θ, and the set of kinematic constraints is finally given by

$$0 < \psi < \pi \tag{23}$$

$$\theta < 2\tan^{-1}(U_k), \quad k = 1, 2 \tag{24}$$

where

$$U_1 = \sqrt{(b\cos\psi - r)/(r + b\sin\psi\sin 2\phi + b\cos\psi\cos 2\phi)}$$

and $U_2 = \sqrt{(r^2 + b^2 - 2br\cos\psi)/(b^2 - r^2)}$.

2) Algorithm for the Maximization of the Volume of the Singularity-Free Workspace With x, y, and ψ Constant: From a methodological perspective, the procedure for the maximization of the volume of the singularity-free region of the workspace with x, y, and ψ constant of the three-leg mechanism is structurally very similar to the one used for the achievement of the first optimum design as described in Section III-C.3. It is described schematically in Fig. 9. Note that, in this case, angle

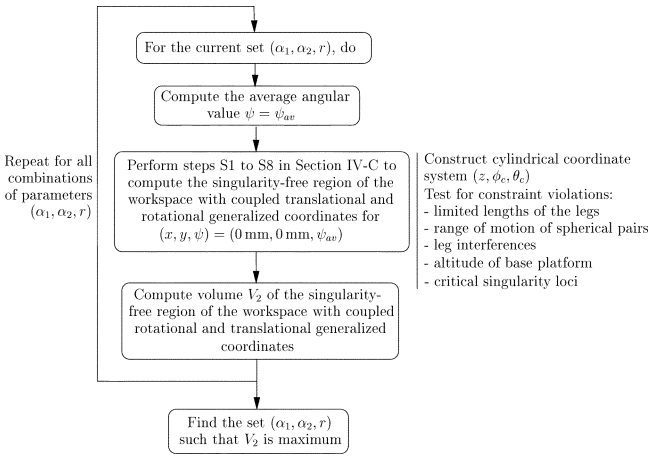

Fig. 9. Flowchart describing the second optimization procedure presented in Section IV-D.2.

ψ_{av} is still computed by (16), in which angle ϕ is substituted by angle ψ in correspondence with the change of orientation parametrization. In the part of the algorithm dedicated to the computation of the workspace, we use

$$z_f = \max_i(\ell_{i1} + \ell_{i5}) + b, \quad i = 1, 2, 3. \tag{25}$$

In addition, the set of constraint checks described by (5), (6), (9), (10), (23), and (24) are applied (more specifically in steps S1 and S4 in Section IV-C) to account for all conventional mechanical constraints and simultaneously ensure that the resulting workspace be free of critical singularities. Finally, for a given set (α_1, α_2, r), the volume of the workspace is computed as follows. Each sector of the workspace is first approximated by a triangular prism defined by four adjacent workspace data points whose volume is easily computed. Then, the volume V_2 of the workspace with x, y, and ψ constant is determined by summing the calculated volumes of all the sectors constituting the upper and lower parts of the workspace.

E. Discussion of Results

This second algorithm was also developed in MATLAB code using data given in the Appendix, with a number of incremental steps $n_\phi = 61, n_\theta = 60$, and $n_z = 150$. Then, we used a procedure similar to the one described in Section III-C.4. We noticed that the maximal value of the volume V_2 of the singularity-free workspace with x, y, and ψ constant is obtained when $\alpha_2 = 30°, (\forall\{\alpha_1, r\})$. Thus, considering the surface defined by $V_2 = f_{\alpha_2}(\alpha_1, r), \alpha_2 = 30°$, we pointed out that a unique local extrema exits with coordinates $r = 280$ mm, i.e., $r = 1.35b$, and $\alpha_1 = 85°$, as shown in Fig. 10. This leads to a maximum volume V_2 equal to 0.245 m·rad^2. The corresponding workspace is graphically represented in Fig. 11. Note, correspondingly, how the representation using the modified Euler angles in a cylindrical coordinate system allowed one to display the workspace as an easy-to-interpret single volume having a simple shape.

Note: The procedure was implemented for the case where $x = y = 0$ mm. However, allowable translational displacements in the x and y directions greater than ± 80 mm were obtained, i.e., $\triangle x = \triangle y = \pm 109$ mm, thus exceeding the desired ranges

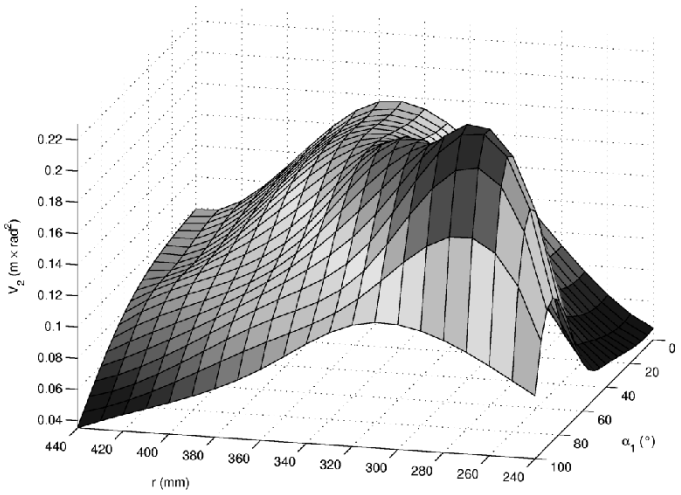

Fig. 10. Volume V_2 as a function of α_1 and $r(\alpha_2 = 30°)$.

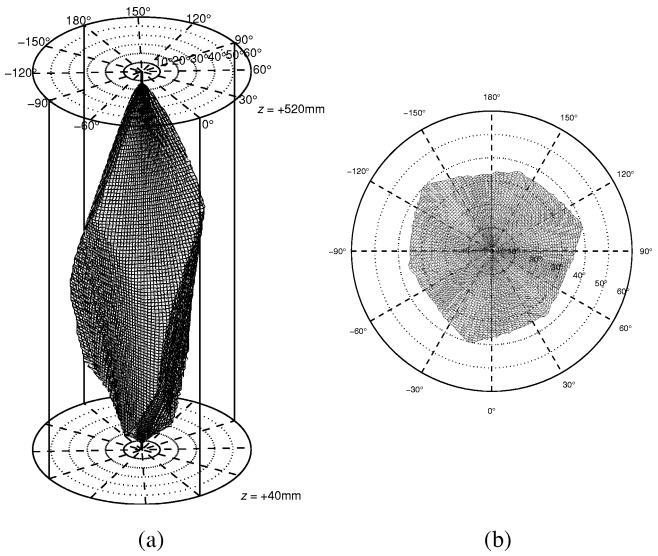

Fig. 11. (a) Perspective and (b) top views of the maximal singularity-free workspace with x, y, and ψ constant $(\alpha_1, \alpha_2, r) = (85°, 30°, 280 \text{ mm}), (x, y, \psi) = (0 \text{ mm}, 0 \text{ mm}, 38°)$.

of possible translations of the platform as provided in Section I for a commercial application of the mechanism as a motion base for flight simulators. If nonsatisfactory allowable displacements had been obtained, an alternative approach consisted in the determination of the optimum set (α_1, α_2, r) such that the average volume $\overline{V}_2 = 1/(n_x n_y) \sum_{\triangle x} \sum_{\triangle y} V_2(x, y, \psi_{\text{av}})$ be maximum, where $\triangle x = \triangle y = \pm 80$ mm and n_x and n_y are the number of discrete intervals over $\triangle x$ and $\triangle y$, respectively.

The design characteristics associated with the initial version of the prototype and those obtained after we conducted the two optimization procedures are summarized in Table I. Taking these results into consideration, and comparing them with the requirements imposed by the two potential applications of the three-leg mechanism, we can make the following observations.

1) The workspace-based kinematic optimizations were successfully implemented without affecting the static balancing-related constraints.
2) Both optimized designs exhibit increased workspace capabilities and kinematic performances. In both cases, the volume of the resulting complete workspace is much larger than the one for the initial prototype and is also free of critical singularity loci.
3) For both industrial applications considered, the fact of optimizing a 3-D particular subset of the complete workspace was proved to be of great interest as it allowed one to obtain design characteristics and inherent workspace capabilities that are especially dedicated to that commercial application. Moreover, the prediction of singular configurations is included at an early stage during the design process and, hence, guarantees no loss of controllability of the architecture during any future trajectory tracking.

V. Conclusion

This paper presented a workspace-based kinematic optimization of a class of three-leg 6-DOF parallel mechanisms that is statically balanced. Considering a possible industrial application of the architecture as a positioning and orienting device of heavy loads, a procedure for the maximization of the volume of the 3-D singularity-free region of the constant-orientation workspace of the mechanism was first presented. As the mechanism could also have great potential as a motion base for flight simulators, we developed a discretization method for the computation of a new workspace with coupled translational and rotational DOFs. This algorithm was the core of a second procedure for the maximization of the volume of the singularity-free region of this second subset of the complete workspace. Both optimization procedures led to very satifactory design characteristics corresponding to enhanced workspace and kinematic properties of the mechanism.

Though applied here to a class of statically balanced parallel manipulators, which involved the choice of a very specific set of design parameters and constraint checks equations, the algorithms presented in Sections III-C.3 and IV-D.2 are, in fact, intrinsically applicable to any type of balanced or nonbalanced spatial parallel manipulator for virtually any set of design parameters, as long as their field of application involves the maximization or either the constant-orientation workspace or the workspace with x, y, and ψ constant; and the equations for their critical singularity loci are known in closed form.

It was finally decided to modify the prototype in accordance with the results of the first optimization (see Fig. 12). As future work will address the real-time control and analysis of the performances of the prototype when dynamically solicited, this mechanism with increased translational ranges of motion will constitute a perfect experimental test bed.

Appendix
Data for the Prototype

Table II shows the data for the initial version of the mechanism. In addition, $\beta_i = 35°, \ell_{i1} = \ell_{i2} = 180$ mm, $\ell_{i5} = 360$ mm, for $i = 1, 2, 3, \alpha_1 = 0°^*, \alpha_2 = 45°^*, r = 280$ mm*, and $b = 207$ mm (the symbol $(^*)$ indicates that the design variable corresponds to the initial version of the prototype).

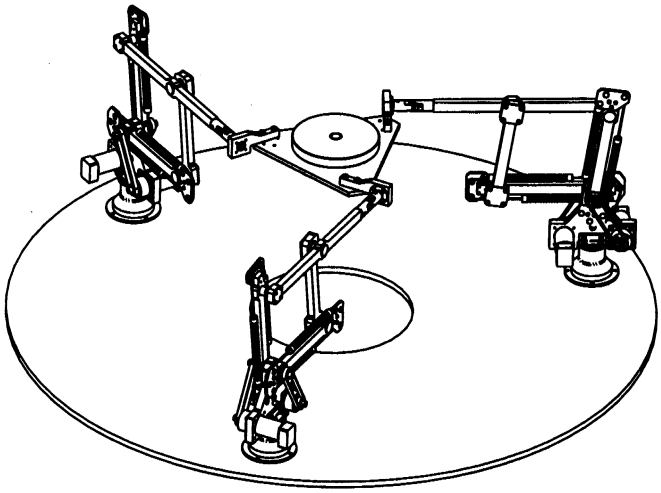

Fig. 12. Final version of the three-leg statically balanced parallel mechanism (CAD model by Dr. J. Wang and P.-L. Richard).

TABLE II
GEOMETRY OF THE INITIAL PROTOTYPE (ALL UNITS ARE IN MILLIMETERS)

i	$\mathbf{p}_{i0}{}^*$	$\mathbf{b}_i$	$\mathbf{j}'_{P_{i5}}{}^*$
1	$\begin{bmatrix} 140.000 \\ -242.487 \\ 0.000 \end{bmatrix}$	$\begin{bmatrix} 103.923 \\ -180.000 \\ 0.000 \end{bmatrix}$	$\begin{bmatrix} 0.354 \\ -0.612 \\ -0.707 \end{bmatrix}$
2	$\begin{bmatrix} 140.000 \\ 242.487 \\ 0.000 \end{bmatrix}$	$\begin{bmatrix} 103.923 \\ 180.000 \\ 0.000 \end{bmatrix}$	$\begin{bmatrix} 0.354 \\ 0.612 \\ -0.707 \end{bmatrix}$
3	$\begin{bmatrix} -280.000 \\ 0.000 \\ 0.000 \end{bmatrix}$	$\begin{bmatrix} -207.000 \\ 0.000 \\ 0.000 \end{bmatrix}$	$\begin{bmatrix} -0.707 \\ 0.000 \\ -0.707 \end{bmatrix}$

ACKNOWLEDGMENT

The authors wish to thank T. Laliberté for his advice concerning design issues.

REFERENCES

[1] T. Arai, T. Tanikawa, J.-P. Merlet, and T. Sendai, "Development of a new parallel manipulator with fixed linear actuator," in *Proc. Japan/USA Symp. Flexible Automation*, vol. 1, Boston, MA, 1996, pp. 145–149.

[2] L. Birglen, C. M. Gosselin, N. Pouliot, B. Monsarrat, and T. Laliberté, "SHaDe, a new spherical haptic device," *IEEE Trans. Robot. Automat.*, vol. 18, pp. 166–175, Apr. 2002.

[3] I. A. Bonev and J. Ryu. Orientation workspace analysis of 6-DOF parallel manipulators. presented at *Proc. ASME Design Engineering Tech. Conf.* [CD-ROM]

[4] I. A. Bonev and C. Gosselin, "Advantages of the modified Euler angles in the design and control of PKMs," in *Proc. 2002 Parallel Kinematic Machines Int. Conf.*, Chemnitz, Germany, 2002, pp. 171–188.

[5] R. Boudreau and C. M. Gosselin, "The synthesis of planar parallel manipulators with a genetic algorithm," *ASME J. Mech. Des.*, vol. 121, no. 4, pp. 533–537, 1999.

[6] R. Boudreau and C. M. Gosselin, "La synthèse d'une plate-forme de Gough–Stewart pour un espace atteignable prescrit," *Mech. Mach. Theory*, vol. 36, no. 3, pp. 327–342, 2001.

[7] M. Ceccarelli and E. Ottaviano. An analytical design for CaPaMan with prescribed position and orientation. presented at *Proc. ASME Design Engineering Tech. Conf.* [CD-ROM]

[8] J. P. Conti, C. M. Clinton, G. Zhang, and A. J. Wavering. (1997) Dynamic variation of the workspace of an octahedral hexapod machine tool during machining. Inst. Syst. Res., Univ. Maryland, College Park, MD. [Online]. Available: http://www.isr.umd.edu/TechReports/ISR/1997/TR_97-28.phtml

[9] I. Ebert-Uphoff and C. M. Gosselin. Kinematic study of a new type of spatial parallel platform mechanism. presented at *Proc. ASME Design Engineering Tech. Conf.* [CD-ROM]

[10] I. Ebert-Uphoff, C. M. Gosselin, and T. Laliberté, "Static balancing of spatial parallel platform mechanisms—Revisited," *ASME J. Mech. Des.*, vol. 122, no. 1, pp. 43–51, 2000.

[11] C. M. Gosselin and J. Angeles, "The optimum kinematic design of a planar three-degree-of-freedom parallel manipulator," *ASME J. Mech., Transmissions, Automat. Des.*, vol. 110, no. 1, pp. 35–41, 1988.

[12] C. M. Gosselin and J. Angeles, "The optimum kinematic design of a spherical three-degree-of-freedom parallel manipulator," *ASME J. Mech., Transmissions, Automat. Des.*, vol. 111, no. 2, pp. 202–207, 1989.

[13] C. M. Gosselin, "Determination of the workspace of 6-DOF parallel manipulators," *ASME J. Mech. Des.*, vol. 112, no. 2, pp. 331–337, 1990.

[14] C. M. Gosselin and J. Angeles, "A global performance index for the kinematic optimization of robotic manipulators," *ASME J. Mech. Des.*, vol. 113, no. 3, pp. 220–226, 1991.

[15] C. M. Gosselin, E. Lavoie, and P. Toutant, "An efficient algorithm for the graphical representation of the three-dimensional workspace of parallel manipulators," *ASME Robot., Spatial Mech., Mech. Syst.*, vol. DE-45, pp. 323–328, 1992.

[16] C. M. Gosselin and E. Lavoie, "On the kinematic design of spherical three-degree-of-freedom parallel manipulators," *Int. J. Robot. Res.*, vol. 12, no. 4, pp. 394–402, 1993.

[17] C. M. Gosselin, J. Wang, T. Laliberté, and I. Ebert-Uphoff, "On the design of a statically balanced 6-DOF parallel manipulator," in *Proc. IFToMM 10th World Congr. Theory of Machines and Mechanisms*, Oulu, Finland, 1999, pp. 1045–1050.

[18] C. M. Gosselin and J. Wang, "Static balancing of spatial six-degree-of-freedom parallel mechanisms with revolute actuators," *J. Robot. Syst.*, vol. 17, no. 3, pp. 159–170, 2000.

[19] J. L. Herder and G. J. M. Tuijthof. Two spatial gravity equilibrators. presented at *Proc. ASME Design Engineering Tech. Conf.* [CD-ROM]

[20] T. Huang, J. Wang, and C. M. Gosselin, "Determination of closed form solution for the 2-D orientation workspace of Gough–Stewart parallel manipulators," *IEEE Trans. Robot. Automat.*, vol. 15, pp. 1121–1125, Dec. 1999.

[21] K. Johnson, "Development of a Statically Balanced Parallel Platform Manipulator," M.S. thesis, Woodruff School of Mech. Eng., Georgia Inst. Technol., Atlanta, GA, 2000.

[22] K. Johnson and I. Ebert-Uphoff, "Development of a spatial statically balanced parallel platform mechanism," in *Proc. 2000 Parallel Kinematic Machines Int. Conf.*, Ann Arbor, MI, 2000, pp. 143–159.

[23] M. Leblond and C. M. Gosselin. Static balancing of spatial and planar parallel manipulators with prismatic actuators. presented at *Proc. ASME Design Engineering Tech. Conf.* [CD-ROM]

[24] O. Ma and J. Angeles, "Optimum architecture design of platform manipulators," in *Proc. 5th Int. Conf. Advanced Robotics*, vol. 2, Pisa, Italy, 1991, pp. 1130–1135.

[25] O. Masory and J. Wang, "Workspace evaluation of Stewart platforms," in *Proc. ASME Design Engineering Tech. Conf.*, vol. 45, Scottsdale, AZ, 1992, pp. 337–346.

[26] J.-P. Merlet, "Détermination de l'espace de travail d'un robot parallèle pour une orientation constante," *Mech. Mach. Theory*, vol. 29, no. 8, pp. 1099–1133, 1994.

[27] ——, "Designing a parallel manipulator for a specific workspace," *Int. J. Robot. Res.*, vol. 16, no. 4, pp. 545–556, 1997.

[28] ——, *Parallel Robots*. Dordrecht, The Netherlands: Kluwer, 2000.

[29] B. Monsarrat and C. M. Gosselin, "Singularity analysis of a three-leg six-degree-of-freedom parallel platform mechanism based on Grassmann line geometry," *Int. J. Robot. Res.*, vol. 20, no. 4, pp. 312–326, 2001.

[30] E. Ottaviano and M. Ceccarelli. Optimal design of CaPaMan (Cassino parallel manipulator) with prescribed position and orientation workspace. presented at *Proc. 9th Int. Conf. Control and Automation*. [CD-ROM]

[31] ——, "Optimal design of CaPaMan (Cassino parallel manipulator) with prescribed orientation workspace," *Robotica*, vol. 20, pp. 159–166, 2002.

[32] V. Parenti-Castelli and R. Di Gregorio, "Workspace and optimal design of pure translation parallel manipulators," in *Proc. 14th Italian Nat. Congress AIMETA*, Paper 65, Como, Italy, 1999, pp. 203–214.

[33] D. A. Streit and B. J. Gilmore, "Perfect spring equilibrators for rotatable bodies," *ASME J. Mech., Transmission, Automat. Des.*, vol. 111, no. 4, pp. 451–458, 1989.

[34] D. Streit, "Spatial manipulator and six-degree-of-freedom platform spring equilibrator theory," in *Proc. 2nd Nat. Conf. Applied Mechanisms and Robotics*, vol. VIII.B, 1991, pp. 1-1–1-6.

[35] J. Wang, "Kinematic analysis, dynamic analysis and static balancing of planar and spatial parallel mechanisms or manipulators with revolute actuators," Ph.D. dissertation, Laval Univ., Quebec City, QC, Canada, 1998.

Bruno Monsarrat received the B.Eng. degree in mechatronics from the École Nationale Supérieure des Arts et Industries de Strasbourg (ENSAIS), Strasbourg, France in 1999 and the Master's degree in mechanical engineering from Laval University, Quebec City, QC, Canada, in 2001.

Between February 2001 and April 2002, he was a Research Engineer in the Robotics Laboratory of the Mechanical Engineering Department, Laval University. His research focused on the design, simulation, and control of parallel robotic manipulators. He is currently a Research Officer with the Automation, Robotics and Intelligent Manufacturing Systems Group of the Aerospace Manufacturing Technology Centre, NRC Institute for Aerospace Research, Montreal, QC, Canada.

Mr. Monsarrat is a member of the Ordre des Ingenieurs du Quebec (OIQ), and a member of the Canadian Committee for the Theory of Machines and Mechanisms (CCToMM).

Clément Gosselin (S'88–M'89) received the B.Eng. degree in mechanical engineering from the Université de Sherbrooke, Sherbrooke, QC, Canada, in 1985, and the Ph.D. degree from McGill University, Montréal, QC, Canada in 1988.

In 1988, he accepted a post-doctoral fellowship from the French government and joined INRIA, Sophia Antipolis, France, for a year. In 1989, he joined the Department of Mechanical Engineering, Laval University, Quebec City, QC, Canada, where he has been a Full Professor since 1997. He has held a Canada Research Chair on Robotics and Mechatronics since January 2001. In 1995, he received a fellowship from the Alexander von Humboldt Foundation which allowed him to spend six months as a Visiting Researcher in the Institut für Getriebetechnik und Maschinendynamik, Technische Hochschule, Aachen, Germany. In 1996, he spent three months at the University of Victoria, Victoria, BC, Canada, for which he received a fellowship from the BC Advanced Systems Institute. His research interests are kinematics, dynamics, and control of robotic mechanical systems with a particular emphasis on the mechanics of grasping and the kinematics and dynamics of parallel manipulators and complex mechanisms. His work in the aforementioned areas has been the subject of several publications in international conferences and journals. He is the French language editor for the international journal *Mechanism and Machine Theory*.

Dr. Gosselin received the Gold Medal of the Governor General of Canada in 1985, the D. W. Ambridge Award from McGill University for the best thesis of the year in Physical Sciences and Engineering in 1988, and the I. Ω. Smith award from the Canadian Society of Mechanical Engineering in 1993. He is a member of the Institute for Robotics and Intelligent Systems (IRIS), one of the networks of the Canadian Centres of Excellence, and a member of the American Society of Mechanical Engineers and the Canadian Committee for the Theory of Machines and Mechanisms (CCToMM).